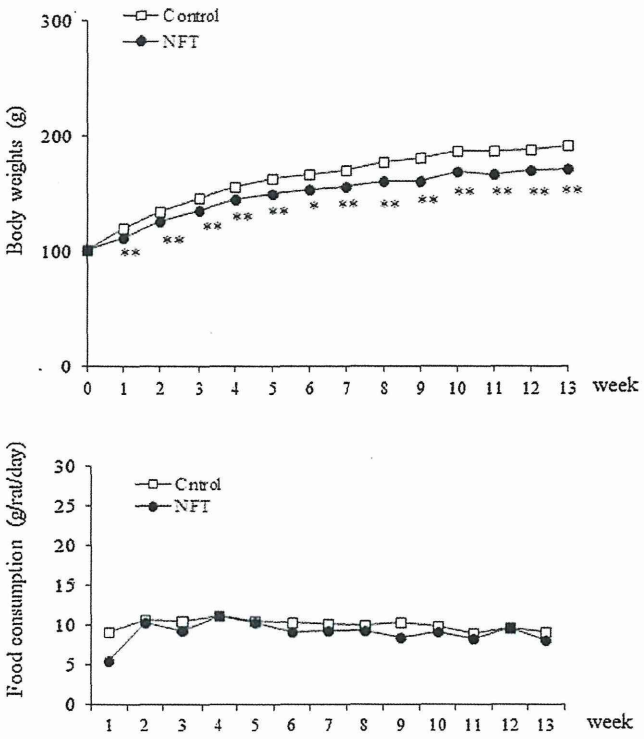

Fig. 5. Growth curves and food consumption for female *gpt* delta rats treated with NFT for 13 weeks. *,** Significantly different ($P < 0.05$, 0.01) from the control group by Student's *t*-test or the Wilcoxon rank sum test.

Table 9
Final body and kidney weights of female *gpt* delta rats treated with NFT for 13 weeks.

	Final body weight (g)	Kidney weight	
		Absolute (g)	Relative (g%)[a]
Control	191.0 ± 11.1[b]	1.10 ± 0.07	0.58 ± 0.03
NFT	171.4 ± 6.3**	1.23 ± 0.08**	0.72 ± 0.05**

[a] Kidney weight-to-body weight ratios (relative weights) are given as g organ weight/g body weight.
[b] Means ± SD.
** Significantly different ($P < 0.01$) from the control group by Student's *t*-test.

transversion mutations, were observed in female rat kidneys similar to the results with males, as shown in Table 11. Results of the Spi⁻ assay are shown in Table 12, with no significant changes in Spi⁻ MF observed in NFT-treated rats.

3.2.3. Measurement of 8-OHdG in kidney DNA

Fig. 6 shows that 8-OHdG levels in the kidneys of female rats treated with NFT for 13 weeks significantly increased to over 5 fold the level of the control group.

4. Discussion

Administration of NFT to male *gpt* delta rats at a dose corresponding to the renal carcinogenic dose in male F344 rats caused a significant increase in *gpt* MFs, but not Spi⁻ MFs, in their kidneys in a dose period-dependent manner. The significant increment of MF in the reporter gene at the carcinogenic target site strongly suggests involvement of genotoxic mechanisms in NFT-induced renal carcinogenesis. In a spectrum analysis of *gpt* mutants in NFT-treated rats, G:C-T:A and G:C-C:G transversion were the predominant mutations found. The guanine base in genomic DNA is highly responsive to various ROS and is susceptible to oxidative modification (Cheng et al., 1992; Kino and Sugiyama, 2000). In fact, 8-OHdG levels in the kidneys of NFT-treated rats were significantly increased after 4 weeks and were further elevated at 13 weeks. The present data clearly demonstrates that NFT at the carcinogenic dose is capable of generating oxidative stress leading to oxidative DNA damage at the carcinogenic target site. Considering that 8-OHdG causes G:C-T:A transversion mutations resulting from its potential for mispairing with adenine (Cheng et al., 1992), oxidative DNA damage including 8-OHdG formation might contribute to guanine base substitution mutations observed in the *gpt* gene following NFT exposure. Since contribution of 8-OHdG to carcinogenicity has been demonstrated (Umemura et al., 2006), genotoxic mechanisms including oxidative DNA damage may be involved in NFT-induced renal carcinogenesis.

Most nitro compounds, such as nitroquinone and nitroheterocycles like nitroimidazole and nitrofurans, are considered to exert their toxic effect by nitro reduction (Bartel et al., 2009; Boelsterli et al., 2006; Chung et al., 2011). One-electron reduction of the nitro group catalyzed by nitro-reductase gives rise to nitro anion radical, the chemical instability of which promotes production of various ROS such as superoxide anion and hydroxyl radical via its electron-donating ability (Wang et al., 2008). It has been reported that the modes of action underlying DNA damage or cytotoxicity induced by NFT in rodent liver and lungs may involve ROS generation by nitro reduction (Rossi et al., 1988; Suntres and Shek, 1992). Accordingly, it is highly probable that nitro reduction

Table 10
gpt MFs in the kidneys of female *gpt* delta rats treated with NFT for 13 weeks.

Treatment	Animal No.	Cm^R colonies ($\times 10^5$)	6-TG^R and Cm^R colonies	MF ($\times 10^{-5}$)	Mean ± SD
Control	1	3.11	6	1.93	
	2	8.10	5	0.62	
	3	5.36	6	1.12	
	4	2.97	3	1.01	
	5	5.99	4	0.67	1.07 ± 0.53
NFT	6	2.88	22	7.64	
	7	N.D.	–	–	
	8	1.89	13	6.88	
	9	5.04	27	5.36	
	10	2.97	17	5.72	6.40 ± 1.05**

Cm^R, chloramphenicol resistant; 6-TG^R 6-thioguanine resistant; MF, mutant frequency; and N.D., not detected.
** Significantly different ($P < 0.01$) from the control group by Student's *t*-test.

Table 11
Mutation spectra of female *gpt* delta rats treated with NFT for 13 weeks.

	Control		NFT	
	Number (%)	Specific mutation frequency ($\times 10^{-5}$)	Number (%)	Specific mutation frequency ($\times 10^{-5}$)
Base substitution				
Transversions				
G:C-T:A	3(13.0)	0.10 ± 0.15	12(22.6)	1.01 ± 0.96*
G:C-C:G	1(4.3)	0	14(26.4)	1.18 ± 0.48*
A:T-T:A	1(4.3)	0.04 ± 0.08	2(3.8)	0.26 ± 0.53
A:T-C:G	3(13.0)	0	2(3.8)	0.26 ± 0.53
Transitions				
G:C-A:T	8(34.8)	0.31 ± 0.08	10(18.9)	0.87 ± 0.51*
A:T-G:C	2(8.7)	0.10 ± 0.15	4(7.5)	0.34 ± 0.30
Deletion				
Single bp	4(17.4)	0.18 ± 0.28	5(9.4)	0.34 ± 0.46
Over 2 bp	0	0	0	0
Insertion	0	0	1(1.9)	0.07 ± 0.10
Complex	1(4.3)	0	3(5.7)	0.29 ± 0.32
Total	23	1.01	53	4.81

* Significantly different ($P < 0.05$) from the control group by Student's *t*-test.

of NFT is responsible for oxidative stress inducing oxidative DNA damage and subsequent gene mutations.

On the other hand, NFA, a constituent compound of NFT with the nitro group, was also able to induce a significant elevation of *gpt* MFs in the kidneys. However, NFA failed to increase 8-OHdG levels in the kidney DNA of *gpt* delta rats despite possessing the same nitro group as NFT. In addition, the mutation spectrum of *gpt* mutants obtained from kidney DNA in NFA-treated rats was not identical to that of NFT-treated rats. NFA has been used as a raw material for the synthesis of many nitrofurans (Cerecetto et al., 1998; Zorzi et al., 2014). Although NFA is known as a photolysis breakdown product from NFT (Busker et al., 1988; Busker and Beijersbergen van Henegouwen, 1987), it is unclear whether NFA could be a metabolite of NFT detected by *in vivo* study.

In general, the rate of nitro reduction is thought to be partly dependent on chemical structure. The inconsistent results between NFT and NFA regarding 8-OHdG formation might indicate that ROS form more readily from the nitro group of NFT. Nitro compounds are reduced to amines as the inactive form via the reactive intermediates including nitroso and hydroxylamine derivatives at multiple stages (Boelsterli et al., 2006). The fact that these reactive intermediates can directly cause nucleophilic reactions with DNA (Cerecetto and González, 2011 Hall et al., 2011; Ona et al., 2009; Streeter and Hoener, 1988) might provide a clue to explaining how NFA induces genotoxicity without oxidative DNA damage. In light of the present data that the other derivative of NFT, AHD, induced neither elevation of 8-OHdG levels nor *gpt* MFs in kidney DNA of rats, it is highly probable that NFA contains a key structural element responsible for NFT-induced genotoxicity. Namely, the mechanisms underlying NFT-induced genotoxicity may involve not only oxidative stress arising from reduction of nitro group, but also some other modes of action involved in the genotoxicity of NFA.

In the NFT-treated group, the accumulation of hyaline droplets in the proximal tubules of the kidney was a prominent feature. Immunohistochemical staining showed these droplets to be positive for α_{2u}-globulin. Western blot analysis also supported NFT being able to accumulate α_{2u}-globulin protein in the proximal tubules. It is well known that the accumulation of α_{2u}-globulin causes the proximal tubular cell injury and subsequently compensatory cell proliferation (Borghoff et al., 2001). Under conditions of the sustained high cell proliferation, it is thought that the rate of spontaneous DNA replication errors is increased (Cunningham, 1996). As a matter of fact, this is the rationale for carcinogenicity of non-genotoxic carcinogens with α_{2u}-globulin inducible potency. In addition, it has been accepted that genomic DNA in cells recruiting into the cell cycle is susceptible to DNA damage. Accordingly, the positive outcome in the reporter gene mutation assay using male rats does not always imply direct genotoxicity of NFT. Therefore, a further study using female *gpt* delta rats, in which the effects of α_{2u}-globulin were not involved, was performed to assess *in vivo* genotoxicity of NFT together with induction of oxidative DNA damage. As a result, administration of NFT to female *gpt* delta rats at the same dose used for males caused significant elevations of both 8-OHdG levels and *gpt* MFs to the same extent as for males. These data clearly showed that α_{2u}-globulin-mediated nephropathy due to NFT treatment did not affect susceptibility to NFT-induced genotoxicity. According to the carcinogenicity studies of NFT conducted by the NTP (1989), NFT was not carcinogenic to the kidneys of female rats in contrast to male rats. Accordingly, α_{2u}-globulin-mediated nephropathy may be a prerequisite for compelling initiated cells to develop neoplastic cells in NFT-induced renal carcinogenesis, *i.e.*, NFT could be a latent carcinogen in female rats, which implies that the cancer hazard to humans still exists.

Table 12
Spi⁻ MFs in the kidneys of female *gpt* delta rats treated with NFT for 13 weeks.

Treatment	Animal No.	Plaques within XL-1 Blue MRA($\times 10^5$)	Plaques within WL95 (P2)	MF ($\times 10^{-5}$)	Mean ± SD
Control	1	7.47	4	0.54	
	2	9.09	3	0.33	
	3	7.56	6	0.79	
	4	6.75	1	0.15	
	5	8.46	4	0.47	0.46 ± 0.24
NFT	6	4.14	5	1.21	
	7	3.69	2	0.54	
	8	6.30	3	0.48	
	9	6.30	2	0.32	
	10	5.04	2	0.40	0.59 ± 0.36

MF, mutant frequency.

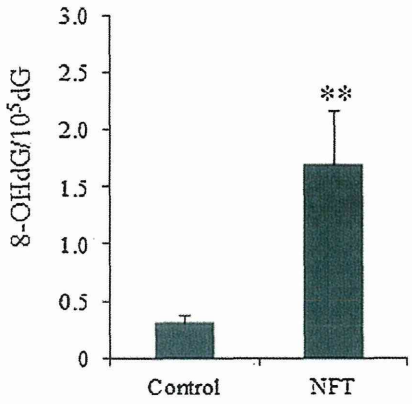

Fig. 6. 8-OHdG levels in the kidneys of female F344 *gpt* delta rats treated with NFT for 4 weeks. Values are means ± SD for 5 rats. ** Significantly different ($P < 0.01$) from the control group by Student's *t*-test.

5. Conclusion

The present study clearly demonstrated that genotoxic mechanisms were involved in NFT-induced renal carcinogenesis in rats. Among the two chemical structure-related compounds of NFT, the common structure between NFT and NFA may play a key role in NFT-induced genotoxicity and not the AHD substructure. The modes of action underlying NFT-induced genotoxicity involve not only NFA-induced genotoxic mechanisms but also oxidative DNA damage. NFT-induced carcinogenicity in rat kidney requires male rat-specific α_{2u}-globulin-mediated nephropathy, but NFT-induced genotoxicity probably occur any species. Therefore, the carcinogenic risk of NFT to humans should be of concern.

Conflict of interest

The authors declare that there are no conflicts of interest.

Transparency document

The Transparency document associated with this article can be found in the online version.

Acknowledgements

We are grateful to members of the department of pathology in NIHS for helpful support. We thank Ms. Ayako Saikawa and Ms. Yoshimi Komatsu for expert technical assistance in processing histological materials. This research was supported by a Grant-in-Aid from the Ministry of Health, Labour and Welfare, Japan (H-22-shokuhin-ippan-007, H25-shokuhin-ippan-005).

References

Bartel, L.C., Montalto de Mecca, M., Castro, J.A., 2009. Nitroreductive metabolic activation of some carcinogenic nitro heterocyclic food contaminants in rat mammary tissue cellular fractions. Food. Chem. Toxicol. 47, 140–144.

Boelsterli, U.A., Ho, H.K., Zhou, S., Leow, K.Y., 2006. Bioactivation and hepatotoxicity of nitroaromatic drugs. Curr. Drug. Metab. 7, 715–727.

Borghoff, S.J., Prescott, J.S., Janszen, D.B., Wong, B.A., Everitt, J.I., 2001. Alpha 2u-globulin nephropathy, renal cell proliferation, and dosimetry of inhaled tert-butyl alcohol in male and female F-344 rats. Toxicol. Sci. 61, 176–186.

Busker, R.W., Beijersbergen van Henegouwen, G.M., 1987. Cytotoxicity and induction of repairable DNA damage by photoactivated 5-nitrofurfural. Toxicology 45, 103–112.

Busker, R.W., Beijersbergen van Henegouwen, G.M., Menke, R.F., Vasbinder, W., 1988. Formation of methemoglobin by photoactivation of nitrofurantoin or of 5-nitrofurfural in rats exposed to UV-A light. Toxicology 51, 255–266.

Cerecetto, H., Di Maio, R., Ibarruri, G., Seoane, G., Denicola, A., Peluffo, G., Quijano, C., Paulino, M., 1998. Synthesis and anti-trypanosomal activity of novel 5-nitro-2-furaldehyde and 5-nitrothiophene-2-carboxaldehyde semicarbazone derivatives. Farmaco 53, 89–94.

Cerecetto, H., González, M., 2011. Antiparasitic prodrug nifurtimox: revisiting its activation mechanism. Future Microbiol. 6, 847–850.

Cheng, K.C., Cahill, D.S., Kasai, H., Nishimura, S., Loeb, L.A., 1992. 8-Hydroxyguanine, an abundant form of oxidative DNA damage, causes G—T and A—C substitutions. J. Biol. Chem. 267, 166–172.

Chung, M.C., Bosquesi, P.L., dos Santos, J.L., 2011. A prodrug approach to improve the physico-chemical properties and decrease the genotoxicity of nitro compounds. Curr. Pharm. 17, 3515–3526.

Cunningham, M.L., 1996. Role of increased DNA replication in the carcinogenic risk of nonmutagenic chemical carcinogens. Mutat. Res. 365, 59–69.

Fleck, L.E., North, E.J., Lee, R.E., Mulcahy, L.R., Casadei, G., Lewis, K., 2014. A screen for a validation of prodrug antimicrobials. Antimicrob. Agents Chemother. 58, 1410–1419.

Hai, A., Kizilbash, N.A., 2013. α(2)-μ-Globulin fragment (a2-f) from kidneys of male rats. Bioinformation 145–149.

Hall, B.S., Bot, C., Wilkinson, S.R., 2011. Nifurtimox activation by trypanosomal type I nitroreductases generates cytotoxic nitrile metabolites. J. Biol. Chem. 286, 13088–13095.

Hiraku, Y., Sekine, A., Nabeshi, H., Midorikawa, K., Murata, M., Kumagai, Y., Kawanishi, S., 2004. Mechanism of carcinogenesis induced by a veterinary antimicrobial drug, nitrofurazone, via oxidative DNA damage and cell proliferation. Cancer Lett. 25, 141–150.

IARC Working Group, 1974. Furaltadone. IARC Monographs on the Evaluation of Carcinogenic Risks to Humans, vol. 7. IARC Working Group, Lyon, France, pp. 161–169.

IARC Working Group, 1983. Furazolidone. IARC Monographs on the Evaluation of the Carcinogenic Risk to Humans, vol. 31. IARC Working Group, Lyon, France, pp. 141–151.

IARC Working Group, 1990a. Nitrofural (nitrofurazone). IARC Monographs on the Evaluation of the Carcinogenic Risks of Chemicals to Humans, vol. 50. IARC Working Group, Lyon, France, pp. 195–209.

IARC Working Group, 1990b. Nitrofurantoin. IARC Monographs on the Evaluation of the Carcinogenic Risks to Humans, vol. 50. IARC Working Group, Lyon, France, pp. 211–231.

Jin, X., Tang, S., Chen, Q., Zou, J., Zhang, T., Liu, F., Zhang, S., Sun, C., Xiao, X., 2011. Furazolidone induced oxidative DNA damage via up-regulating ROS that caused cell cycle arrest in human hepatoma G2 cells. Toxicol. Lett. 201, 205–212.

Kino, K., Sugiyama, H., 2000. GC–>CG transversion mutation might be caused by 8-oxoguanine oxidation product. Nucleic Acids Symp. Ser. 44, 139–140.

Maaland, M., Guardabassi, L., 2011. In vitro antimicrobial activity of nitrofurantoin against *Escherichia coli* and *Staphylococcus pseudintermedius* isolated from dogs and cats. Vet. Microbiol. 151, 396–399.

Matsushita, K., Ishii, Y., Takasu, S., Kuroda, K., Kijima, A., Tsuchiya, T., Kawaguchi, H., Miyoshi, N., Nohmi, T., Ogawa, K., Nishikawa, A., Umemura, T., 2015. A medium-term gpt delta rat model as an in vivo system for analysis of renal carcinogenesis and the underlying mode of action. Exp. Toxicol. Pathol. 67, 31–39.

McCalla, D.R., 1983. Mutagenicity of nitrofuran derivatives: review. Environ. Mutagen. 5, 745–765.

National Toxicology Program (NTP), 1989. NTP Toxicology and Carcinogenesis Studies of nitrofurantoin (CAS No. 67-20-9) in F344/N rats and B6C3F1 mice (Feed Studies). Natl. Toxicol. Program Tech. Rep. Ser. 341, 12–18.

Nohmi, T., Suzuki, T., Masumura, K., 2000. Recent advances in the protocols of transgenic mouse mutation assays. Mutat. Res. 20, 191–215.

Ona, K.R., Courcelle, C.T., Courcelle, J., 2009. Nucleotide excision repair is a predominant mechanism for processing nitrofurazone-induced DNA damage in *Escherichia coli*. J. Bacteriol. 191, 4959–4965.

Quillardet, P., Arrault, X., Michel, V., Touati, E., 2006. Organ-targeted mutagenicity of nitrofurantoin in Big Blue transgenic mice. Mutagenesis 21, 305–311.

Rossi, L., Silva, J.M., McGirr, L.G., O'Brien, P.J., 1988. Nitrofurantoin-mediated oxidative stress cytotoxicity in isolated rat hepatocytes. Biochem. Pharmacol. 37, 3109–3117.

Streeter, A.J., Hoener, B.A., 1988. Evidence for the involvement of a nitrenium ion in the covalent binding of nitrofurazone to DNA. Pharm. Res. 5, 434–436.

Suntres, Z.E., Shek, P.N., 1992. Nitrofurantoin-induced pulmonary toxicity. In vivo evidence for oxidative stress-mediated mechanisms. Biochem. Pharmacol. 43, 1127–1135.

Umemura, T., Kai, S., Hasegawa, R., Kanki, K., Kitamura, Y., Nishikawa, A., Hirose, M., 2003. Prevention of dual promoting effects of pentachlorophenol, an environmental pollutant, on diethylnitrosamine-induced hepato- and cholangiocarcinogenesis in mice by green tea infusion. Carcinogenesis 24, 1105–1109.

Umemura, T., Kanki, K., Kuroiwa, Y., Ishii, Y., Okano, K., Nohmi, T., Nishikawa, A., Hirose, M., 2006. In vivo mutagenicity and initiation following oxidative DNA lesion in the kidneys of rats given potassium bromate. Cancer Sci. 97, 829–835.

Wagenlehner, F.M., Wullt, B., Perletti, G., 2011. Antimicrobials in urogenital infections. Int. J. Antimicrob. Agents 38, 3–10.

Wang, Y., Gray, J.P., Mishin, V., Heck, D.E., Laskin, D.L., Laskin, J.D., 2008. Role of cytochrome P450 reductase in nitrofurantoin-induced redox cycling and cytotoxicity. Free Radic. Biol. Med. 44, 1169–1179.
Wang, Y., Shia, M.A., Christensen, T.G., Borkan, S.C., 2000. Hepatic alpha 2 mu-globulin localizes to the cytosol of rat proximal tubule cells. Kidney Int. 57, 1015–1026.
Williams, G.M., Jeffrey, A.M., 2000. Oxidative DNA damage: endogenous and chemically induced. Regul. Toxicol. Pharmacol. 32, 283–292.
Zorzi, R.R., Jorge, S.D., Palace-Berl, F., Pasqualoto, K.F., Bortolozzo Lde, S., de Castro Siqueira, A.M., Tavares, L.C., 2014. Exploring 5-nitrofuran derivatives against nosocomial pathogens: synthesis, antimicrobial activity and chemometric analysis. Bioorg. Med. Chem. 22, 5844–5852.

Research article

Journal of Applied Toxicology

Received: 29 November 2014, Revised: 8 March 2015, Accepted: 17 March 2015 Published online in Wiley Online Library: 22 May 2015

(wileyonlinelibrary.com) DOI 10.1002/jat.3163

Onset of hepatocarcinogen-specific cell proliferation and cell cycle aberration during the early stage of repeated hepatocarcinogen administration in rats

Masayuki Kimura[a,b], Hajime Abe[a,b], Sayaka Mizukami[a,b], Takeshi Tanaka[a,b], Megu Itahashi[a,b], Nobuhiko Onda[a], Toshinori Yoshida[a] and Makoto Shibutani[a]*

ABSTRACT: We have previously reported that a 28-day treatment of carcinogens evoking target cell proliferation activates G_1/S checkpoint function and apoptosis, as well as induction of aberrant ubiquitin D (Ubd) expression, suggesting disruptive spindle checkpoint function, in rats. The present study aimed to determine the onset time of rat liver cells to undergo carcinogen-specific cell cycle aberration and proliferation. Animals were treated orally with a hepatocarcinogenic dose of methyleugenol or thioacetamide for 3, 7 or 28 days. For comparison, some animals were subjected to partial hepatectomy or treated with noncarcinogenic hepatotoxicants (acetaminophen, α-naphthyl isothiocyanate or promethazine). Carcinogen-specific liver cell kinetics appeared at day 28 as evident by increases of cell proliferation, $p21^{Cip1+}$ cells, phosphorylated-$Mdm2^+$ cells and cleaved caspase 3^+ cells, and upregulation of DNA damage-related genes. Hepatocarcinogens also downregulated *Rbl2* and upregulated *Cdkn1a* and *Mdm2*, and decreased Ubd^+ cells co-expressing phosphorylated-histone H3 (p-Histone H3) and p-Histone $H3^+$ cell ratio within the Ki-67^+ proliferating population. These results suggest that it takes 28 days to induce hepatocarcinogen-specific early withdrawal of proliferating cells from M phase due to disruptive spindle checkpoint function as evidenced by reduction of Ubd^+ cells staying at M phase. Disruption of G_1/S checkpoint function reflected by downregulation of *Rbl2* as well as upregulation of *Mdm2* suggestive of sequestration of retinoblastoma protein is responsible for the facilitation of carcinogen-induced cell proliferation at day 28. Accumulation of DNA damage probably in association with facilitation of p53 degradation by activation of Mdm2 may be a prerequisite for aberrant $p21^{Cip1}$ activation, which is responsible for apoptosis. Copyright © 2015 John Wiley & Sons, Ltd.

Keywords: cell proliferation; hepatocarcinogen; G_1/S checkpoint; spindle checkpoint; ubiquitin D; apoptosis

Introduction

Carcinogenicity assays using rodent animals are versatile for evaluating the carcinogenic potential of test compounds. However, they have several disadvantages, such as long duration, high costs and use of a large number of animals. Although there are a number of alternative models, e.g., two-stage carcinogenesis bioassays (Tamano, 2010) and bioassays using genetically modified animals by transgenic or gene targeting technologies (Eastin, 1998), they are also expensive and time-consuming, and have limited target organs. Toxicogenomic approaches for the prediction of carcinogenic potential in each target organ appear promising; however, they are also expensive and require integrative methodologies between different laboratories sharing expression databases (Uehara *et al.*, 2011). Therefore, the development of new and rapid means for evaluation or prediction of the carcinogenic potential of chemicals in the whole body is necessary for efficient detection of carcinogens.

The development of nuclear enlargement is sometimes observed in carcinogenic target cells after repeated administration of carcinogens, irrespective of genotoxic potential, from the early stages of exposure in rodents (Adler *et al.*, 2009; Allen *et al.*, 2004). This nuclear enlargement is typically observed in the liver and kidney. It has been reported that renal carcinogens are classified into two categories, the renal tubular nephropathy type and the renal tubular karyomegaly-inducing type (Taniai *et al.*, 2012a). Recent studies have shown that ochratoxin A, a renal carcinogen in rodents, can induce karyomegaly, which reflects mitotic disruption and subsequent unstable polyploidy, accompanied by aberrant expression of cell cycle-related molecules, particularly, of G_2 and M phases (Adler *et al.*, 2009). Hepatocarcinogens at the early stage of carcinogenicity bioassays frequently induce hepatocellular cytomegaly/karyomegaly (Allen *et al.*, 2004) suggesting that induction of cell cycle aberration is an early stage signature of carcinogen responses. It has also been reported that escape from

* *Correspondence to: Makoto Shibutani, Laboratory of Veterinary Pathology, Tokyo University of Agriculture and Technology, 3-5-8 Saiwai-cho, Fuchu-shi, Tokyo 183-8509, Japan.*
E-mail: mshibuta@cc.tuat.ac.jp

[a] *Laboratory of Veterinary Pathology, Tokyo University of Agriculture and Technology, Fuchu-shi, Tokyo, Japan*

[b] *Pathogenetic Veterinary Science, United Graduate School of Veterinary Sciences, Gifu University, Gifu-shi, Gifu, Japan*

the G_2/M checkpoint along with the accumulation of DNA damage during cell proliferation may lead to chromosomal mis-segregation and cytokinesis failure, causing tetraploidy/aneuploidy and subsequent chromosomal instability (Ichijima *et al.*, 2010). We therefore hypothesize that an early event, which disrupts cell cycle regulation, triggers the carcinogenic response in the molecular mechanism responsible for the development of cytomegaly/karyomegaly.

We have recently found that carcinogens evoking cell proliferation in carcinogenic target cells after a 28-day administration can also induce aberrant expression of cell cycle-related molecules reflecting activation of G_1/S checkpoint function and apoptosis in many target organs (Taniai *et al.*, 2012a, b; Yafune *et al.*, 2013a, b). Furthermore, by double immunohistochemical analysis, we found that ochratoxin A, targeting renal tubular cells and thioacetamide (TAA), targeting liver cells, induce aberrant expression of ubiquitin D (Ubd), at G_2 phase, suggestive of disruption of the spindle checkpoint at M phase (Taniai *et al.*, 2012b). These results suggest that cell proliferation-inducing carcinogens induce aberrant cell cycle regulation including dysfunction of M phase players, indicating the early cellular events responsible for the carcinogenicity. However, the cellular onset time point of carcinogen-specific cellular proliferation has not been addressed until now.

The present study was performed to identify the cellular onset time point of carcinogen-specific facilitation of aberrant cell cycle during the early time course of repeated carcinogen administration. For this purpose, we repeatedly administered hepatocarcinogens to rats for up to 28 days and examined the temporal changes in cell proliferation activity, expression of G_1/S and spindle checkpoint-related molecules and apoptosis by immunohistochemistry and real-time reverse transcription–polymerase chain reaction (RT-PCR). For comparison, we also examined the liver cell responses under regenerative cell proliferation induced by partial hepatectomy or non-carcinogenic hepatotoxicants.

Materials and methods

Chemicals

Methyleugenol (MEG; CAS no. 93-15-2, purity ≥ 98.0%), acetaminophen (APAP; CAS no. 103-90-2, purity ≥ 98.0%) and α-naphthyl isothiocyanate (ANIT; CAS no. 551-06-4, purity ≥ 98.0%) were purchased from Tokyo Chemical Industry Co. (Tokyo, Japan). TAA (CAS no. 62-55-5, purity > 98%), promethazine hydrochloride (PMZ; CAS no. 58-33-3, purity > 98%) and methylcellulose 400 were purchased from Wako Pure Chemicals Industries (Osaka, Japan).

Animal experiments

Five-week-old male F344/NSlc rats were purchased from Japan SLC, Inc. (Shizuoka, Japan), and acclimatized to a powdered basal diet (CRF-1; Oriental Yeast Co., Tokyo, Japan) and tap water ad libitum for 1 week. Rats were maintained under standard conditions (room temperature, 23 ± 3 °C; relative humidity, 50 ± 20%; 12 h light/dark cycle).

In the present study, two lines of animal experiments were conducted. In both experiments, animals were subjected to two-thirds partial hepatectomy or to administration of hepatocarcinogens (MEG or TAA) or noncarcinogenic hepatotoxicants (APAP, ANIT or PMZ). MEG and TAA were selected as hepatocarcinogens (Becker, 1983; NTP, 2000), and APAP, ANIT and PMZ were selected as non-carcinogenic hepatotoxicants (NTP, 1993a, b; Rees *et al.*, 1962). Three- and 7-day repeated administration studies were conducted in experiment 1, and a 28-day repeated administration study was conducted in experiment 2. In both experiments, cell proliferation activity, expression of cell cycle-related molecules and apoptosis were examined using immunohistochemistry, and gene expression changes in cell cycle molecules, signaling molecules and repair enzymes were examined by real-time RT-PCR.

Experiment 1

Animals were divided into seven groups based on initial body weights and subjected to a two-thirds partial hepatectomy (PH, $n = 22$), or exposed to MEG (1000 mg kg^{-1} body weight) daily by gavage in 0.5% methylcellulose ($n = 22$), TAA (400 ppm) in basal diet ($n = 20$), APAP (10 000 ppm) in basal diet ($n = 20$), ANIT (1000 ppm) in basal diet ($n = 20$) or PMZ (200 mg kg^{-1} body weight) daily by gavage in 0.5% methylcellulose ($n = 22$) for 3 or 7 days. Untreated controls ($n = 20$) were maintained on the basal diet and tap water without any treatment during the experimental period. In the PH group, one animal died at day 6 after PH treatment. In the ANIT group, the animals' body weights decreased at day 3 after the start of treatment, so the dose was reduced to 600 ppm thereafter. In the PMZ group, the animals' body weights decreased at day 3 after the start of treatment, so the dose was reduced to 100 mg kg^{-1} body weight. One day after the 3- and 7-day treatment period, half of the animals in each group were killed by exsanguination from the abdominal aorta under deep anesthesia with CO_2/O_2 and livers were removed.

Experiment 2

Animals were divided into seven groups based on initial body weights and subjected to PH ($n = 12$), or exposed to MEG (1000 mg kg^{-1} body weight) daily by gavage in 0.5% methylcellulose ($n = 11$), TAA (400 ppm) in basal diet ($n = 10$), APAP (10 000 ppm) in basal diet ($n = 10$), ANIT (600 ppm) in basal diet ($n = 11$) or PMZ (100 mg kg^{-1} body weight) by gavage in 0.5% methylcellulose ($n = 11$) for 28 days. Untreated controls ($n = 10$) were maintained on the basal diet and tap water without any treatment during the experimental period. In the MEG group, one animal was killed at day 10 after the start of treatment, because of its deteriorating general condition, and then the dose was reduced from 1000 to 800 mg kg^{-1} body weight. One day after the 28-day treatment period, all animals were killed by exsanguination from the abdominal aorta under deep anesthesia with CO_2/O_2 and livers were removed.

The dose levels of MEG and TAA selected in both experiments even after the dose change were reported to be tumor-inducible (Becker, 1983; NTP, 2000). The initial dose levels of APAP, ANIT and PMZ induced hepatotoxicity after a 13- or 16-week administration in rats (NTP, 1993a, b; Rees *et al.*, 1962).

The animal protocols were reviewed and approved by the Animal Care and Use Committee of the Tokyo University of Agriculture and Technology. All efforts were made to minimize animal suffering.

Histology and immunohistochemistry

Three-micrometer sections of paraffin-embedded tissues from the liver were stained with hematoxylin and eosin for histopathological examination, or subjected to immunohistochemistry. Immunohistochemistry of liver sections was performed using the Vectastain® Elite ABC Kit (Vector Laboratories Inc., Burlingame, CA, USA) with 3,3'-diaminobenzidine/H_2O_2 as the chromogen and antibodies against the following proteins: Ki-67, a cell proliferation marker expressed in the nucleus during the G_1 to M phase of

the cell cycle (Scholzen & Gerdes, 2000), cleaved caspase 3, an apoptosis marker expressed during the later stage of apoptosis (Eckle *et al.*, 2004), Topollα, acting on DNA decatenation at G_2/M phase (Mattila *et al.*, 2007), phosphorylated histone H3 (p-Histone H3), acting on chromatin condensation at the early M phase (Hirota *et al.*, 2005), Mad2, a spindle checkpoint protein (Kops *et al.*, 2004), phosphorylated histone H2AX (γH2AX), which responds to DNA damage (Burma *et al.*, 2001), $p21^{Cip1}$, one of the cyclin-dependent kinase inhibitors (Sherr & Roberts, 1995), and Ubd, a molecule that leads to chromosomal instability through reduction in kinetochore localization of checkpoint proteins, such as Mad2, during the G_2/M phase (Herrmann *et al.*, 2007; Lim *et al.*, 2006), phosphorylated Mdm2 (p-Mdm2), a p53 downstream molecule that facilitates degradation of p53 (Malmlöf *et al.*, 2007; Mayo & Donner, 2002). Information of antibodies and their antigens used in experiments are shown in Table 1. Sections were counterstained with hematoxylin for microscope examination. Endogenous peroxidase activity was blocked with 0.3% hydrogen peroxide.

For double immunohistochemistry of Ubd with Topollα or p-Histone H3, 3,3'-diaminobenzidine was used to visualize Ubd with the Vectastain® ABC-AP kit (Vector Laboratories Inc.), and Vector® Red Alkaline Phosphate Substrate Kit I (Vector Laboratories Inc.) was used to visualize Topollα and p-Histone H3.

Analysis of immunoreactivity

The immunoreactive cells for Ki-67, Topollα, p-Histone H3, Ubd, Mad2, γH2AX, $p21^{Cip1}$ or p-Mdm2 were counted in 10 selected areas per animal at 200 × magnification, and the immunoreactive cells for cleaved caspase 3 were counted in five selected areas per animal at 100 × magnification, avoiding areas of connective tissues and vasculature. In case of even distribution of immunoreactive cells, area selection was conducted randomly. In case of uneven immunoreactive cell distribution within the liver lobules, such as accumulation of immunoreactive cells at the periportal area, 5 or 10 adjacent areas were selected for analysis to avoid selection of areas disproportionately. Immunoreactive liver cells were counted visually, and the total number of liver cells in the micrographs was separately counted using the image binarization method in the Win-ROOF image analysis and measurement software (version 6.4.2.; Mitani Corporation, Fukui, Japan). Then, the percentage of total immunoreactive cells was estimated in each animal.

Real-time reverse transcription–polymerase chain reaction analysis

To investigate the expression levels of representative cell cycle-related genes and DNA damage-related genes in the liver, mRNA expression analysis was performed using the StepOnePlus™ Real-time RT-PCR System (Life Technologies, Carlsbad, CA, USA) with the SYBR®Green PCR Master Mix (Life Technologies). The forward and reverse primers listed in Table 2 were designed using the Primer Express 3.0 software (Life Technologies). Using the threshold cycle values of *Hprt1* in the same sample as the endogenous control, the relative differences in gene expression were calculated using the $2^{-\Delta\Delta C}{}_T$ method (Livak & Schmittgen, 2001).

Statistical analysis

All data are represented as mean ± SD. Numerical data were analyzed by the Bartlett's test for the homogeneity of variance. If there was no significant difference in variance, Dunnett's test was performed for comparison between the groups. If a significant difference was found in variance, Steel's test was performed. All numerical data of the treatment groups were compared with those of untreated controls.

Table 1. Antibodies used for immunohistochemistry

Antigen	Abbreviated name	Host species	Clone name	Dilution	Antigen retrieval [a]	Manufacturer (city, state, country)
Ki-67 antigen	Ki-67	Mouse	Monoclonal (MIB-5)	1: 200	Autoclaving in citrate buffer	Dako (Glostrup, Denmark)
Cleaved caspase 3 (Asp175)	-	Rabbit	Polyclonal	1: 500	Autoclaving in target retrieval solution	Cell Signaling Technology, Inc. (Danvers, MA, USA)
$p21^{Cip1}$	-	Mouse	Monoclonal (CP74)	1: 1000	Microwaving in citrate buffer	Abcam (Cambridge, UK)
Ubiquitin D	Ubd	Rabbit	Polyclonal	1: 400	Autoclaving in citrate buffer	Proteintech Group, Inc. (Chicago, IL, USA)
Topoisomerase II alpha	Topollα	Rabbit	Monoclonal (EP1102Y)	1: 400	Autoclaving in citrate buffer	Epitomics, Inc. (Burlingame, CA, USA)
Phosphorylated histone H3 (Ser10)	Phospho-Histone H3	Rabbit	Polyclonal	1: 400	Autoclaving in citrate buffer	Santa Cruz Biotechnology, Inc. (Santa Cruz, CA, USA)
Histone H2AX (phospho-Ser139)	γH2AX	Rabbit	Monoclonal (EP854(2)Y)	1: 1000	Autoclaving in citrate buffer	Abcam
Mitotic arrest deficient-2	MAD2	Mouse	Monoclonal (48/MAD2)	1: 400	Microwaving in citrate buffer	BD Transduction Laboratories (Lexington, KY, USA)
Phosphorylated Mdm2 (Ser166)	p-Mdm2	Rabbit	Polyclonal	1: 400	Autoclaving in target retrieval solution	Cell Signaling Technology, Inc.

[a]Antigen retrieval was applied for immunohistochemistry. Retrieval conditions were either autoclaving at 121 °C for 10 min in 10 mM citrate buffer (pH 6.0) or in target retrieval solution (3-in-1; pH 9.0, Dako), or microwaving at 90 °C for 10 min in 10 mM citrate buffer (pH 6.0).

Table 2. Sequence of primers used for real-time RT-PCR

Gene	Accession no.	Forward primer (5′ → 3′)	Reverse primer (5′ → 3′)
G_1/S checkpoint-related genes			
Cdkn1a	NM_080782	ACCAGCCACA GGCACCAT	CGGCATACTT TGCTCCTGTG T
Cdkn2a	NM_031550	CAAACGCCCC GAACACTT	CACTTTGACG TTGCCCATCA
Rb1	NM_017045	CACCAGGCCT CCTACCTTGT C	AGGAATCCGC AAGGGTGAAC
Rbl2	NM_031094	AAGTGAATCG CCTGCAAAAA G	CTCGGTCATT AGCTACATCT TGGA
Mdm2	NM_001108099	GAAGGAGGAC ACACAAGACA AAGA	ATGGCTCGAT GGCGTTCA
Tp53	NM_030989	CATGAGCGTT GCTCTGATGG T	GATTTCCTTC CACCCGGATA A
Spindle checkpoint and M phase-related genes			
Aurka	NM_153296	AAGAGAGTCA TCCACAGAGA CATCAA	CGATCTTCAA CTCCCCATTT G
Aurkb	NM_053749	CGGATGCATA ATGAGATGGT AGAT	TCCCCACCAT CAGTTCATAG C
Bub1	NM_001106507	CCCTAGCTCC CAGTCCTAAA AGT	TTGTGGAATG GTGTAGATGA AAGC
Mad1l1	NM_001109387	TCCAGGAGTT CCGCAAGGT	GAGGCGGTAT TGGCTCTCAG T
Mad2l1	NM_001106594	ACAGCCACTG TGACATTTCT ACCA	CCCGATTCTT CCCACTTTTC A
Plk1	NM_017100	TCCCACCAAG GTTTTCAATA GC	TGTGAGAGGC TTCCTGTTGC T
DNA damage-related genes			
Atm	NM_001106821	AGGCTGTCGG CAGGTGTTT	TGGTGTACGG CGTATCTTTG C
Brca1	AF036760	TGATGTGGGA CTGGGTGTTG	CTGTACCAGG TAGGCATCCA GAT
Brca2	NM_031542	AGGCTTTCGG TTGGCAGAT	AGAGACCCAG ACGCTAGAAA TCA
Brcc3	NM_001127300	CCACATCCAC TCGGTCATCA T	AAATCTCCAC GCGGTCCTT
Chek1	NM_080400	TGGCAGCTGG CAAAGGA	AATCCCAGTC TTCCACAAAA GG
Chek2	NM_053677	TTGCTTCGAT GGACCACTGT T	GATGCGAAAG TGCTTCTTGC T
Esco1	NM_001126299	CCAAATCCCA CTGCCGTTA	GCTGCCTCTT TTGCTCTTTC C
Gadd45a	NM_024127	CACCATAACT GTCGGCGTGT A	GGCACAGGAC CACGTTGTC
Rad17	NM_001024778	GACTGGGTAG ATCCGGCATT T	AAACGGTGAT GGTGGTGACA
Rad50	NM_022246	TGGCCCCTGG CAGTGA	AACTTCGCAC GCCCAGAGT
Housekeeping gene			
Hprt1	NM_012583	GCCGACCGGT TCTGTCAT	TCATAACCTG GTTCATCATC ACTAATC

Atm, ATM serine/threonine kinase; Aurka, aurora kinase A; Aurkb, aurora kinase B; Brca1, breast cancer 1, early onset; Brca2, breast cancer 2, early onset; Brcc3, BRCA1/BRCA2-containing complex, subunit 3; Bub1, BUB1 mitotic checkpoint serine/threonine kinase; Cdkn1a, cyclin-dependent kinase inhibitor 1A; Cdkn2a, cyclin-dependent kinase inhibitor 2A; Chek1, checkpoint kinase 1; Chek2, checkpoint kinase 2; Esco1, establishment of sister chromatid cohesion N-acetyltransferase 1; Gadd45a, growth arrest and DNA-damage-inducible, alpha; Hprt1, hypoxanthine phosphoribosyltransferase 1; Mad1l1, MAD1 mitotic arrest deficient-like 1 (yeast); Mad2l1, MAD2 mitotic arrest deficient-like 1 (yeast); Mdm2, MDM2 proto-oncogene, E3 ubiquitin protein ligase; Plk1, polo-like kinase 1; RAD17, RAD17 homolog (S. pombe); Rad50, RAD50 homolog (S. cerevisiae); Rb1, retinoblastoma 1; Rbl2, retinoblastoma-like 2; RT-PCR, reverse transcription–polymerase chain reaction; Tp53, tumor protein p53.

Results

Body and liver weight

At day 3, the final body weights significantly decreased in the PH, MEG, TAA, ANIT and PMZ groups, compared with untreated controls (Table 3). The absolute liver weight after PH was significantly lower than untreated controls. The absolute liver weights of rats in the MEG and APAP groups were significantly higher than untreated controls. The relative liver weights of rats in the MEG, TAA, APAP, ANIT and PMZ groups were significantly higher than untreated controls.

At day 7, the body weights significantly decreased in all treatment groups, compared with untreated controls (Table 3). The absolute liver weights of rats in the PH and ANIT groups were significantly lower than untreated controls. The relative liver weights of rats in the MEG, TAA, APAP, ANIT and PMZ groups were significantly higher than untreated controls.

At day 28, the body weights significantly decreased in the MEG, TAA, APAP, ANIT and PMZ groups compared with untreated controls (Table 3). The absolute liver weights of rats in the PH, TAA and ANIT groups were significantly lower than untreated controls. The absolute liver weight of rats in the PMZ group was significantly higher than untreated controls. The relative liver weights of rats in the MEG, TAA, APAP, ANIT and PMZ groups were significantly higher than untreated controls.

Histopathological changes

MEG treatment revealed no apparent histopathological changes at day 3, centrilobular liver cell hypertrophy associated with cytoplasmic ground glass appearance at day 7 and diffused distribution of liver cells showing cytomegaly and anisokaryosis at day 28, as previously reported (NTP, 2000). TAA treatment caused centrilobular liver cell hypertrophy associated with nucleolar enlargement at days 3 and 7, and periportal vacuolar degeneration of liver cells at day 7. At day 28, TAA treatment resulted in diffused liver cell cytomegaly often associated with anisokaryosis, aberrant mitosis, and apoptosis and periportal oval cell proliferation, as previously

Table 3. Initial and final body weights and liver weight of rats after partial hepatectomy, or after treatment with hepatocarcinogens or hepatotoxicants

Group	Number of animals	Initial body weight (g)	Final body weight (g)	Liver weight	
				Absolute (g)	Relative (g 100 g^{-1} BW)
Day 3 (experiment 1)					
CONT	10	123.8± 3.8[a]	147.7 ± 5.1	6.40 ± 0.31	4.33 ± 0.13
PH	11	121.3 ± 4.4	124.5 ± 4.9**	3.91 ± 0.38**	3.14 ± 0.22
MEG	11	121.8 ± 4.7	129.0 ± 5.4**	6.92 ± 0.36*	5.37 ± 0.24**
TAA	10	123.0 ± 6.7	134.3 ± 4.9**	6.39 ± 0.36	4.76 ± 0.18**
APAP	10	122.2 ± 2.7	142.1 ± 4.5	6.94 ± 0.54*	4.88 ± 0.25**
ANIT	10	122.4 ± 3.0	125.8 ± 4.0**	6.28 ± 0.43	4.99 ± 0.27**
PMZ	11	121.2 ± 4.4	118.3 ± 9.0**	6.03 ± 0.44	5.11 ± 0.38**
Day 7 (experiment 1)					
CONT	10	124.2 ± 9.9	167.4 ± 13.9	6.95 ± 0.71	4.15 ± 0.14
PH	10	121.1 ± 10.4	141.8 ± 9.0**	5.19 ± 0.65**	3.66 ± 0.34
MEG	11	122.7 ± 10.0	139.4 ± 5.8**	7.21 ± 0.42	5.17 ± 0.30**
TAA	10	122.7 ± 7.4	141.5 ± 8.0**	7.21 ± 0.38	5.10 ± 0.19**
APAP	10	123.3 ± 8.4	150.4 ± 12.0**	6.82 ± 0.88	4.52 ± 0.29*
ANIT	10	123.1 ± 8.2	121.7 ± 5.4*	5.71 ± 0.36**	4.70 ± 0.23**
PMZ	11	121.0 ± 9.4	136.2 ± 7.1**	7.22 ± 0.42	5.30 ± 0.29**
Day 28 (experiment 2)					
CONT	10	128.0 ± 7.8	250.8 ± 10.5	10.20 ± 0.48	4.07 ± 0.14
PH	12	128.1 ± 5.3	240.5 ± 10.2	9.40 ± 0.52*	3.91 ± 0.07
MEG	10	128.3 ± 5.8	186.0 ± 16.3**	10.54 ± 1.20	5.65 ± 0.22**
TAA	10	126.9 ± 7.3	152.4 ± 10.4**	7.71 ± 0.79**	5.05 ± 0.30**
APAP	10	127.4 ± 5.9	218.6 ± 8.6**	9.48 ± 0.62	4.33 ± 0.13**
ANIT	11	126.3 ± 7.2	162.8 ± 11.3**	8.79 ± 0.64**	5.40 ± 0.16**
PMZ	11	126.7 ± 6.8	212.4 ± 13.2**	11.39 ± 0.90**	5.36 ± 0.20**

ANIT, α-naphthyl isothiocyanate; APAP, acetaminophen; CONT, untreated controls; MEG, methyleugenol; PH, partial hepatectomy; PMZ, promethazine hydrochloride; TAA, thioacetamide.
[a]Values are expressed as mean ± SD.
* $P < 0.05$, ** $P < 0.01$ vs. untreated controls (Dunnett's or Steel's test).

reported (Clawson *et al.*, 1992). Nucleolar enlargement was apparent in these cytomegalic cells at this time point. Treatment with APAP revealed no apparent histopathological changes at day 3. In contrast, APAP treatment for 7 or 28 days revealed slight centrilobular liver cell hypertrophy, as previously reported (NTP, 1993a). ANIT treatment resulted in periportal bile duct proliferation from day 3. From day 7, scattered focal liver cell necrosis was observed, as previously reported (Rees *et al.*, 1962). PMZ treatment resulted in centrilobular liver cell hypertrophy and ground glass appearance at day 7 and day 28, as previously reported (NTP, 1993b).

Cell proliferation and apoptosis

Ki-67 was immunolocalized in the nucleus of liver cells (Fig. 1A,C,E). Ki-67$^+$ cells distributed evenly within the liver lobules, except for preferential distribution at the periportal area in the TAA group at days 3 and 7 and in the PMZ group at day 28. Cleaved caspase 3 was immunolocalized in the nucleus and cytoplasm of liver cells (Fig. 1B,D,F). Cleaved caspase 3$^+$ cells preferentially distributed at the periportal area in any group at any time point.

At day 3, the number of Ki-67$^+$ cells significantly increased in the PH, TAA, APAP and ANIT groups and significantly decreased in the PMZ group, compared with untreated controls (Fig. 1A). The number of cleaved caspase 3$^+$ cells significantly increased in the TAA group and significantly decreased in the PMZ group, compared with untreated controls (Fig. 1B).

At day 7, the number of Ki-67$^+$ cells significantly decreased in the PH, APAP and ANIT groups, compared with untreated controls (Fig. 1C). The number of cleaved caspase 3$^+$ cells significantly increased in the MEG, TAA, APAP and ANIT groups, compared with untreated controls (Fig. 1D).

At day 28, the number of Ki-67$^+$ cells significantly increased in the MEG, TAA and PMZ groups, compared with untreated controls (Fig. 1E). The number of cleaved caspase 3$^+$ cells significantly increased in the MEG and TAA groups, compared with untreated controls (Fig. 1F).

Immunoreactive cellular distribution

TopoⅡα, p-Histone H3, Mad2, γH2AX, p21^{Cip1} and p-Mdm2 were immunolocalized in the nucleus of liver cells, and Ubd was immunolocalized in the cytoplasm or mitotic spindle of liver cells (Fig. 2A–G). Immunoreactive cells for TopoⅡα, p-Histone H3, Mad2 and γH2AX distributed evenly within the liver lobules, except for preferential distribution at the periportal area in the TAA group at days 3 and 7 and in the PMZ group at day 28. Immunoreactive cells for p21^{Cip1} and p-Mdm2 preferentially distributed at the periportal area in any group at any time point.

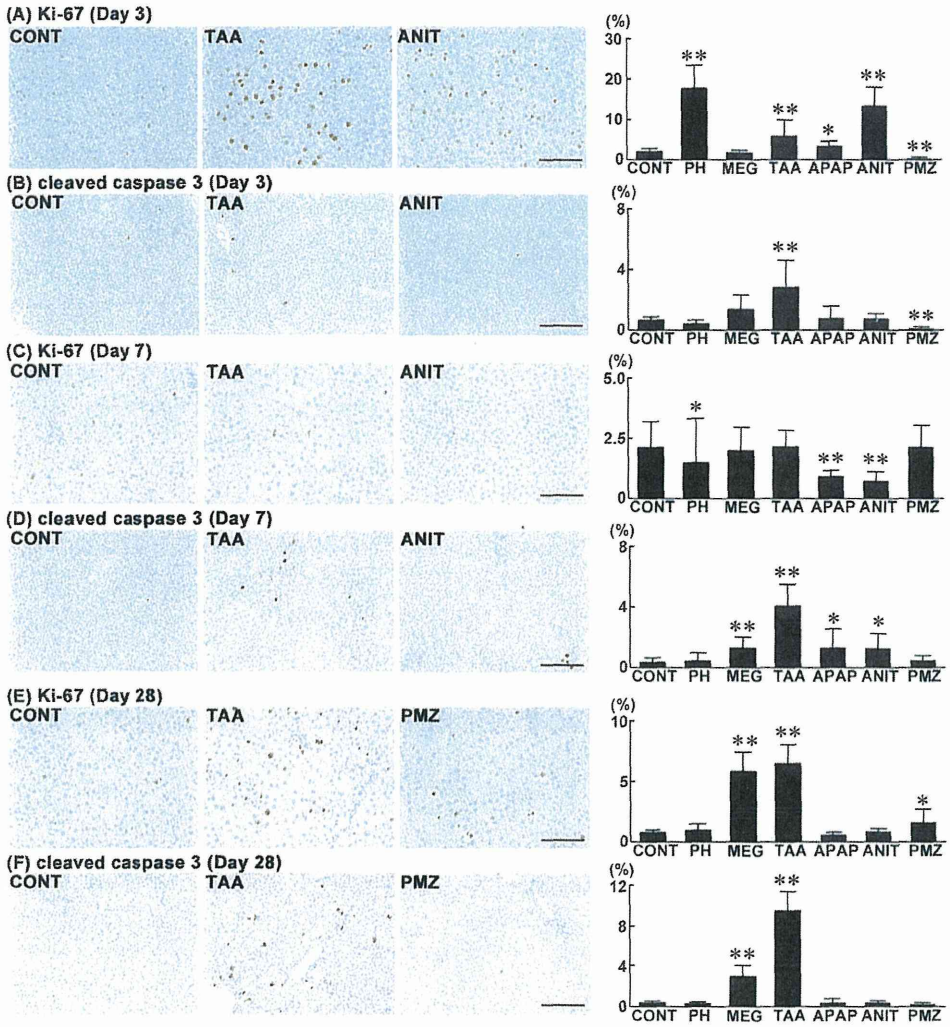

Figure 1. Distribution of Ki-67$^+$ and cleaved caspase 3$^+$ cells in the liver of rats at days 3, 7 and 28 after treatment with PH, noncarcinogenic hepatotoxicants or hepatocarcinogens. Photomicrographs show the distribution of Ki-67$^+$ and cleaved caspase 3$^+$ cells in the liver of representative cases from untreated controls (A–F), animals treated with TAA or ANIT (A–D), and animals treated with TAA or PMZ (E,F). The graphs show the positive cell ratios of hepatocytes per total cells counted in 10 animals in each group. Values represent mean + SD. (A) Ki-67 (day 3), (B) cleaved caspase 3 (day 3), (C) Ki-67 (day 7), (D) cleaved caspase 3 (day 7), (E) Ki-67 (day 28) and (F) cleaved caspase 3 (day 28). Bar = 100 μm (A,C,E) or 200 μm (B,D,F). *$P < 0.05$, **$P < 0.01$ vs. untreated controls (Dunnett's or Steel's test). ANIT, α-naphthyl isothiocyanate; APAP, acetaminophen; CONT, untreated controls; MEG, methyleugenol; PH, partial hepatectomy; PMZ, promethazine hydrochloride; TAA, thioacetamide.

At day 3, the number of TopoⅡα$^+$ cells, p-Histone H3$^+$ cells and Mad2$^+$ cells significantly increased in the PH, TAA and ANIT groups, and significantly decreased in the MEG and PMZ groups, compared with untreated controls (Fig. 2A–C). The number of Ubd$^+$ cells and γH2AX$^+$ cells significantly increased in the PH, TAA and ANIT groups, and significantly decreased in the PMZ group, compared with untreated controls (Fig. 2D,E). The number of p21^{Cip1+} cells significantly increased in the MEG, TAA and APAP groups, compared with untreated controls (Fig. 2F). The number of p-Mdm2$^+$ cells significantly increased in the MEG and TAA groups, compared with untreated controls (Fig. 2G).

At day 7, the number of TopoⅡα$^+$ cells, p-Histone H3$^+$ cells and Mad2$^+$ cells significantly decreased in the PH, MEG, APAP and ANIT groups, compared with untreated controls (Fig. 3A–C). The number of Ubd$^+$ cells significantly decreased in the PH, MEG, TAA, APAP and ANIT groups, compared with untreated controls (Fig. 3D). The number of γH2AX$^+$ cells significantly decreased in the PH, APAP and ANIT groups, compared with untreated controls (Fig. 3E). The number of p21^{Cip1+} cells significantly increased in the MEG, TAA, APAP and ANIT groups, compared with untreated controls (Fig. 3F). The number of p-Mdm2$^+$ cells significantly increased in the MEG, TAA, APAP and PMZ groups, compared with untreated controls (Fig. 3G).

At day 28, the number of TopoⅡα$^+$ cells significantly increased in the PH, MEG, TAA and PMZ groups, and significantly decreased in APAP group, compared with untreated controls (Fig. 4A). The number of p-Histone H3$^+$ cells, Mad2$^+$ cells and γH2AX$^+$ cells significantly increased in the MEG, TAA and PMZ groups, compared with untreated controls (Fig. 4B,C,E). The number of Ubd$^+$ cells significantly increased in the PH, MEG, TAA and PMZ groups, compared with untreated controls (Fig. 4D). The number of p21^{Cip1+} cells significantly increased in the MEG, TAA and APAP groups, compared with untreated controls (Fig. 4F). The number of p-Mdm2$^+$ cells significantly increased in the MEG and TAA groups, compared with untreated controls (Fig. 4G).